Korean J. Chem. Eng., 32(10), 2124-2132 (2015)
DOI: 10.1007/s11814-015-0068-0
pISSN: 0256-1115
eISSN: 1975-7220

Study and characterization of W/Si and W/B4C multilayer for applications in hard X-rays mirror

Chang Kyu Kim*,, Young Sei Park*, Sei Jin Han*, Jang yool Chae*, and Byung-Ki Na**,†**

*Research Center, Hanwha L&C, Sinseong-dong, Yuseong-gu, Daejeon 305-804, Korea
**Department of Chemical Engineering, Chungbuk National University,
52, Naesudong-ro, Heungduk-gu, Cheongju, Chungbuk 362-763, Korea
(*Received 24 May 2014 • accepted 6 April 2015*)

Abstract−Multilayer thin films with 2.3 nm-7.6 nm of d-spacing were deposited on fusion glass and float glass substrates by magnetron sputtering. Multilayer thin film with a lower interface roughness was deposited at an abnormal discharge region of I-V characteristic curve in DC glow discharge, compared to normal discharge region. Interface roughness of periodical multilayer in general depends on layer thickness, but in this study interface roughness was controlled by adjusting deposition conditions regardless of layer thickness. But interface roughness and X-ray reflectivity (XRR) of multilayer react sensitively to surface roughness of substrate. Multilayer thin film with 2.3 nm d-spacing shoes 42% of characteristic X-ray reflectivity(Cu Kα, λ=~0.154 nm), while 3.6 nm d-spacing shows 80% of reflectivity. XRR, transmission electron microscope (TEM) and atomic force microscopy (AFM) were used to analyze the interface roughness (σ), surface roughness and d-spacing.

Keywords: Hard X-ray Mirror, Sputter, X-ray Reflectivity, Multilayer Thin Film, Sputterlattice

INTRODUCTION

A thin film in nm range thickness separated by layers with different atomic number (Z) is called a multilayer. Multilayer thin film was used as an X-ray optics which can reflect hard X-ray. X-ray energy can be artificially selected for properly designing and producing materials with high atomic number (Z), such as W and Mo, and materials with low atomic number (Z) [1-3]. This artificial Bragg reflection has been used as an X-ray mirror in the whole industry such as in medicine and material research.

Unlike general optical microscopes, an X-ray microscope can observe the inside of a material. The magnification of an X-ray microscope is 300x to 10,000x which is between an optical microscope and an electron microscope. Studies on X-ray focusing optics to make an X-ray microscope using a monochromatic X-ray source have been reported [4,5]. The use of a monochromatic X-ray source offers the sensitivity to each chemical element which presents a unique Xray attenuation coefficient.

Studies on X-ray optics were reported by using multilayer mirrors to increase detection limits of a specific element in X-ray fluorescence (XRF) [6]. X-ray optics made from W/Si multilayer is used as an optical system of Grazing incidence X-ray diffraction (GIXRD), because it can analyze micro area or thin layer of the sample [7].

A monochromatic X-ray of a desirable wavelength was used for the medical imaging system and the non-constructive analytical system [8]. When monochromatic X-ray is used in the medical imaging system of angiography or mammography, clear image can be obtained with less exposition to radiation. If X-ray image is photographed at low d-spacing of W/Si and W/B4C multilayer, equal contrast can be obtained irrespective of the thickness of subject.

A multilayer also has been widely used in studies on universe X-ray detection. In the past, universe has been observed at a visible ray region but studies of analyzing images with X-ray and γ-ray have started. Studies on the multilayer have been reported for the analysis of energies of 100 keV or higher [9,10].

Interfacial condition of multilayer is very important to decide the performance of the mirror. Non ideal interfaces reduce the reflectivity. Interface quality is usually determined by the magnitude and lateral character of the interfacial roughness (standard deviation of the interface height), vertical correlation of the roughness for different interface, the thickness of individual layer, and the extent of intermixed layer thickness and its composition. The interfacial characteristics of thin multilayer are the basis of the research of X-ray mirror.

The factors affecting interface structure of multilayer are number of bilayer, value of thickness of period, Γ ratio, the bilayer period length, and deposition method and deposition parameter. The effect of deposition parameters on the interface structure in W/Si and Mo/Si has already been extensively studied and reported by various investigators [11-13].

Deposition parameters were decided to explore the effect of interfacial structure on the multilayer manufacturing. Multilayer with d-spacing of 10 nm or lower by magnetron sputter were synthesized, and Cu characteristics X-ray (CuKα, λ=~0.154 nm) were

†To whom correspondence should be addressed.
E-mail: nabk@chungbuk.ac.kr
Copyright by The Korean Institute of Chemical Engineers.

used to analyze a multilayer structure and X-ray reflection features.

EXPERIMENTS

1. Multilayer Design

An X-ray mirror can be formed by fabricating a multilayer system consisting of layers of different index of refraction. Bragg's law ($n\lambda=2d\sin\theta$) is valid between multilayer thickness and an X-ray incident angle. The Bragg equation is changed to compensate for the refraction in the layers [14]

$$n\lambda=2d_M\sin\theta\sqrt{1-\frac{2\bar{\delta}}{\sin^2\theta}}=2d_M\sin\theta\left(1-\frac{4\bar{\delta}d_M^2}{n^2\lambda^2}\right) \quad (1)$$

with the order n, the wavelength λ, the period d_M of the multilayer system, the angle of incidence θ and the real part $\bar{\delta}$ of the period-averaged index of refraction of the multi layer system.

This effect was not considered in the experiments, because the effect of refraction at Bragg equation could be compensated by controlling the incident angle in case of selecting hard X-ray energy. D-spacing was designed to reflect a hard X-ray with reflection energy of 20-60 keV in the range of an incident angle between 0.2° and 0.4°. Reflected energies in accordance with incident angle and d-spacing calculated by Bragg equation are listed in Table 1. In medical imaging system, 50 keV is used in CT, 35 keV is used in angiography, and 18.5 keV is used in mammography. The energy difference of 1-2 keV can be adjusted by changing the incident angle.

2. Sample Preparation

A magnetron sputter with physical vapor deposition (PVD) using plasma was used for multilayer deposition. The installed target was the 600 mm×110 mm×6 mmT planar target and the distance between a target and a substrate was 40 mm. Purity of W, Si, SiC and B4C was 99.95%, 99.999%, 99.5% and 99.5%, respectively. The B4C target, a non-conductive material, used RF power and the target of the rest of conductive materials used DC power.

After lowering the chamber's base pressure up to 2.0×10^{-7} Torr, Ar gas was inserted up to $1\text{-}3\times10^{-3}$ Torr. 100-2,000 W DC or RF power was supplied and glass substrates shuttled between the W target and the Si (B4C) target for multilayer deposition of 10-60 layers.

A deposition rate was chosen to maintain a ratio of a low atomic number (Z) material to bilayer thickness determined by a multilayer design (Gamma (Γ) Ratio) between 0.4 and 0.6.

$$\text{Gamma}(\Gamma)\text{Ratio}=\frac{\text{Si, B4C Thickness}}{\text{Bilayer Thickness}} \quad (2)$$

Table 1. Reflected energies (keV) in accordance with incident angle (degree) and d-spacing (nm) calculated by Bragg equation

Incident angle (°)	d-Spacing (nm)							
	7.5	7.20	7.0	6.8	3.9	3.8	3.55	2.35
	Reflected energy (keV)							
0.2	24	25	25	26	46	47	50	76
0.25	19	20	20	21	36	37	40	60
0.3	16	16	17	17	30	31	33	50
0.35	14	14	14	15	26	27	29	43
0.4	12	12	13	13	23	23	25	38

In addition, the substrate moving speed should increase for deposition of thin layers of several nanometers in high power. However, it was hard to decrease thickness by only increasing the substrate moving speed. Therefore, a deposition rate was adjusted by installing a mask, an assistance device, between a target and a substrate. Deposition rates of W, Si and B4C were 2.5-3.5 nm/sec, 0.6-1.2 nm/sec and 0.8 nm/sec, respectively.

3. X-ray Reflectivity (XRR) Analysis

XRR analysis was used to determine d-spacing, interface, surface roughness and Cu characteristics X-ray (Cu Kα, λ=~0.154 nm) reflectivity of a multilayer made. Cu was used as an anode material of an X-ray tube. Omega-2theta scan (Specular Scan) between 0 and 6° was conducted in the range of a scan step of 0.002°-0.006° and of each step's time of 2-6 seconds. The fringe period of the reflectivity pattern changed depending on total thickness of a sample. The current and voltage used were 25 mA and 40 kV. Measurement errors due to X-ray beam divergence were minimized using 0.1 mm divergence slit and 0.2 mm receiving slit.

Parratt32 [15] using the Parratt recursion method was used for curve fitting of the XRR measurement result.

Reflectivity of a sample with n thin layers can be obtained by the Parratt recursion method. Total reflectivity r_{j-1}^F in the j−1 interface and j interface for arbitrary layer j are related to r_j^F and F_{j-1} [16,17].

$$r_{j-1}^F=\frac{F_{j-1}+r_j^F\exp(-iq_jt_j)}{1+F_{j-1}r_j^F\exp(-iq_jt_j)} \quad (3)$$

r_j^F is defined as a ratio of a reflected X-ray to an incident X-ray. And r_j^F is called as "a total reflection coefficient in interface j". A boundary condition of Eq. (3) can be obtained from interface n with $r_n^F=F_n$. Therefore, reflectivity of each layer from j=n to r_0^F can be calculated by recursion method of Eq. (3). When measuring XRR, X-ray intensity measured by detector can be calculated by $Rf=|r_0^F|^2$.

However, the mean vertical electron density profile of a sample, which has a non-ideal interface with actual roughness, can be modeled by error function and the Névot-Croce roughness [18]. Therefore, r_j^F in Eq. (3) can be replaced by r_j^{N-C} [17,19].

$$r_j^{N-C}=r_j^F\exp(-2\sigma_j^2k_0^2f_jf_{j+1}) \quad (4)$$

Cu characteristic X-ray (Cu Kα, λ=~0.154 nm) reflectivity of a sample was calculated by dividing photon count (R) of X-rays, reflected by 1st Bragg reflection, by photon count (R0) of incident X-rays.

$$\text{Reflectivity}=\frac{R}{R0} \quad (5)$$

R is the photon count of the 1st peak of XRR measurement raw data and R0 is the photon count measured by an XRR detector in the absence of specimen.

At the low angle of XRR measurement the raw data and curve fit data were not coincident. The area of the sample at the low angle was so small that the incident X-ray could not be reflected. To reduce the X-ray loss at low angle, the sample size should be increased infinitely. The data before critical angle were not related to this exper-

imental scope, so the data were not used.

A cross sectional image of a multilayer produced using TEM was taken and the result was compared with the XRR measurement result.

4. Changes in Substrate Roughness

The effects of substrate roughness on multilayer interface characteristics and X-ray reflectivity were investigated. Multilayers were deposited on fusion glass 0.5 mmT, fusion glass 0.7 mmT and float glass 1.1 mmT with different surface roughness under the same process condition. The surface roughness of fusion glass is lower than the float glass. The surface roughness of substrate was measured with the non-contact mode of AFM, and was scanned on 10 μm×10 μm area.

The W/Si multilayer was deposited on three kinds of substrate to 60 layers with d-spacing of 2.3 nm. Samples were classified into WS230(60)-Fusion 0.5T, WS230(60)-Fusion 0.7T and WS230(60)-Float 1.1T.

5. Comparison of Normal Glow and Abnormal Glow

DC glow discharge has a normal glow region where the current increases and the voltage does not increase as power increases. It has an abnormal glow region where both the current and the voltage increase as power increases [20]. In the normal glow region, a deposition rate is low so that the deposition number is increased to set desirable d-spacing. In the abnormal glow region, a deposition rate is high so that a mask is used to decrease a deposition rate in order to make a sample with desirable d-spacing. The 7.5 nm d-spacing and 3.55 nm d-spacing samples were deposited in the normal and abnormal glow region to compare an interface status.

Table 2. Different deposition conditions of various samples

Sample name	Purpose of test	Different conditions
WS355(25) W/Si 3.55 nm N=25 WS355(20) W/Si 3.35 nm N=20 WS750(10)A W/Si 7.5 nm N=10 WS750(10)B W/Si 7.5 nm N=10	Comparison of normal glow and abnormal glow	Sputter power (current, voltage) Scan speed Scan pass
WSC235(60)-Fusion 0.5T W/SiC2.35 nm N=60 WSC235(60)-Fusion 0.7T W/SiC2.35 nm N=60 WSC235(60)-Float 1.1T W/SiC2.35 nm N=60	Comparison of the effect of substrate surface roughness	Surface roughness of substrate
WS390(20), WS380(20), WS355(20)	Comparison of d-spacing (bilayer thickness)	Deposition rate control using mask width
WB355(30) W/B4C3.55 nm N=30 WB355(60) W/B4C3.55 nm N=60	Sample preparation for maximum reflectivity	Optimized sample preparation

Table 3. Recipe of DC sputter process for fabrication of multilayer thin film

Sample name	Material	Power (KW)	Process pressure (mTorr)	DC current (A)	DC voltage (V)	Ar (sccm)	Carrier speed (cm/min)	Pass	Mask size (mm)
WS355(25) W/Si 3.55 nm N=25	W	DC1.0	3.0	3.46	288	72.7	590	1	X
	Si	DC2.0	3.0	4.26	470	63.6	380	1	X
WS355(20) W/Si 3.35 nm N=20	W	DC2.0	3.0	5.8	344	70.5	310	1	40*110
	Si	DC2.0	3.0	4.22	475	65.6	295	1	110*110
WS750(10)A W/Si 7.5 nm N=10	W	DC0.1	3.0	0.34	287	71.8	800	22	X
	Si	DC0.1	3.0	0.28	352	64.3	800	30	X
WS750(10)B W/Si 7.5 nm N=10	W	DC2.0	1.0	5.68	352	25.1	500	1	X
	Si	DC2.0	1.0	3.08	348	22.4	100	1	X
WSC235(60)-Fusion 0.5T W/SiC2.35 nm N=60	W	DC2	3.0	6.5	308	70.2	290	1	20*144
	SiC	DC2	3.0	5.72	349	66.9	260	1	70*144
WS390(20) WS380(20) WS355(20)	W	DC2	3.0	5.92	338	71.6	300	1	(70-60) *110
	Si	DC2	3.0	6.32	317	66.8	295	1	(40-35) *110
WSC235(60)-Fusion 0.7T WSC235(60)-Float 1.1T W/SiC 2.35 nm N=60	W	DC2	3.0	6.6	303	66.9	290	1	20*144
	SiC	DC2	3.0	5.98	335	64.5	260	1	70*144

Table 4. Recipe of DC and RF sputter process for fabrication of multilayer thin film

Sample name	Material	Power (KW)	Process pressure (mTorr)	DC current (A) / RF power forward (W)	DC voltage (V) / RF power reflect (W)	Ar (sccm)	Carrier speed (cm/min)	Pass	Mask size (mm)
WB355(30) W/B4C3.55 nm N=30	W	DC2.0	3.0	5.96	322	71.1	400	1	40*144
	B4C	RF2.0	10.0	1963	39	252.4	20	1	70*144
WB355(60) W/B4C3.55 nm N=60	W	DC2.0	3.0	6.3	317	76.5	400	1	40*144
	B4C	RF2.0	10.0	1969	35	265.8	20	1	70*144

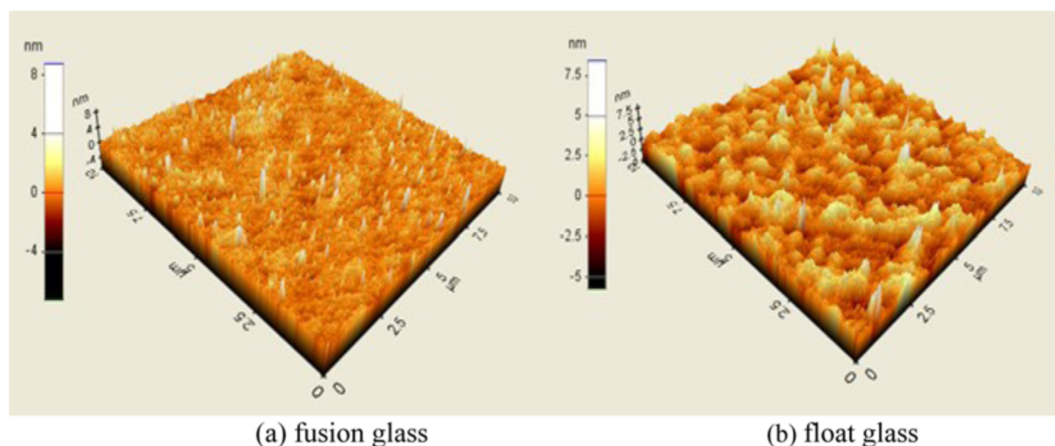

Fig. 1. Surface roughness morphology of substrate: (a) fusion glass with Rms=0.67 nm, (b) float glass with Rms=1.1 nm.

Samples WS750(10)A and WS355(25) were deposited in the normal glow region, and WS750(10)B and WS355(20) were deposited in the abnormal glow region.

6. Changes in d-Spacing

We changed the mask width to make a sample whose d-spacing was changed under the same sputter process condition (W Mask width: 70 mm-60 mm, Si Mask width: 40 mm-35 mm). The substrate moving speed was set as 0.05 m/s for W and 0.049 m/s for Si to make sample WS390(20), WS380(20) and WS355(20) of d-spacing of 3.9-3.55 nm. A sample was produced under the same process condition.

7. Hard X-ray Mirror Production

A multilayer with d-spacing of 3.55 nm was produced to reflect 40 keV X-rays at an incident angle of 0.25° and 50 keV X-rays at an incident angle of 0.20° on fusion glass 0.5 mmT substrates. Samples WB355(30) and WB355(60) had a bilayer of 30 and 60 layers, respectively. Deposition conditions of samples are listed in Table 2. The conditions of DC sputter process for fabrication of multilayer thin film are listed in Table 3. The recipe of DC and RF sputter process is listed in Table 4.

RESULTS AND DISCUSSION

1. Roughness of Substrate

In the result of substrate analysis by atomic force microscopy (AFM), surface roughness of fusion glass 0.5 mmT, fusion glass 0.7 mmT and float glass 1.1 mmT was Rms 0.67 nm, Rms 0.82 nm and Rms 1.1 nm, respectively. The surface of float glass was rougher than that of fusion glass. The morphology (surface shape) of fusion glass 0.5 mmT and float glass 1.1 mmT is shown in Fig. 1.

The result of XRR measurement and analysis after repeated deposition for 60 layers with d-spacing of 2.35 nm on three substrates with different roughness is shown in Fig. 2 and Table 5. Three substrates were fusion glass 0.5 mmT (Rms roughness=0.67 nm), fusion glass 0.7 mmT (Rms roughness=0.82 nm) and float glass 1.1 mmT

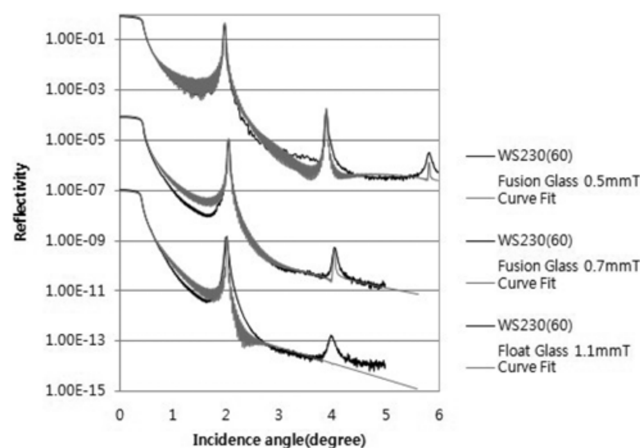

Fig. 2. Grazing incidence X-ray reflectivity of samples WS230(60) deposited on fusion glass 0.5 mmT, fusion glass 0.7 mmT and float glass 1.1 mmT substrate (black line) and optimum curve fitting simulations (gray line) (the parameters of the simulations are listed in Table 4).

Table 5. Parameters for simulations of the X-ray reflectivity from Samples WS230(60) deposited on fusion glass 0.5 mmT, fusion glass 0.7 mmT and float glass 1.1 mmT substrate as shown in Fig. 2 (parameters were obtained by Parratt32 software[16])

Glass	Repetition (N)	d-Spacing (nm)	Gamma (Γ)	Surface Roughness and interface widths (σ) (nm)				Reflectivity of 1st Bragg Peak (%)
				Surface	Si on W	W on Si	Substrate	
Fusion 0.5 mmT	60	2.3	0.50	0.20	0.45	0.39	0.20	41.7
Fusion 0.7 mmT	60	2.2	0.45	0.90	0.53	0.65	0.12	10.3
Float 1.1 mmT	60	2.2	0.45	0.83	0.85	0.75	0.2	1.9

(Rms roughness=1.1 nm). Besides substrate roughness, interface and surface roughness of WS235(60) using fusion glass 0.5 mmT as a substrate was 0.2-0.5 nm. Interface and surface roughness of WS235(60) using fusion glass 0.7 mmT as a substrate was 0.5-0.9 nm. Interface and surface roughness of WS235(60) using float glass 1.1 mmT as a substrate was 0.7-0.9 nm. Therefore, a multilayer deposited on rougher substrate has rougher interface and surface.

In WS235(60) using fusion glass 0.5 mmT, fusion glass 0.7 mmT and float glass 1.1 mmT as substrates, Cu characteristic X-ray reflectivity was 41.7%, 10.3% and 1.9%, respectively. It was confirmed that substrate roughness highly affected interface roughness and X-ray reflectivity of a multilayer.

When a multilayer deposited on a float glass substrate in thickness of 3 mm regardless of a material type was deposited, interface roughness was 900 nm. When Si wafer was used as a substrate, the interface roughness was 0.23-0.25 nm [9].

When a periodical multilayer was deposited on the substrate with non-ideal surface roughness, interface roughness became severe with the increase of deposition because of roughness replication [21,22]. In this study interface and surface roughness of periodical multilayer was controlled by adjusting deposition conditions.

2. Effect of the Sputtering Conditions

In the result of XRR measurement and curve fitting shown in Fig. 3, the 3rd Bragg peak did not accord with curve fitting data in case of WS355(25) because one model was used for simulation during curve fitting. Therefore, a difference in interface roughness between next above substrates and on a layer close to the surface was not reflected as shown in Fig. 4(b). On the other hand, interface roughness next above substrates and on a layer close to the surface was similar in case of WS355(20) as shown in Fig. 4(a). The XRR measurement result accorded with data of one model simulation.

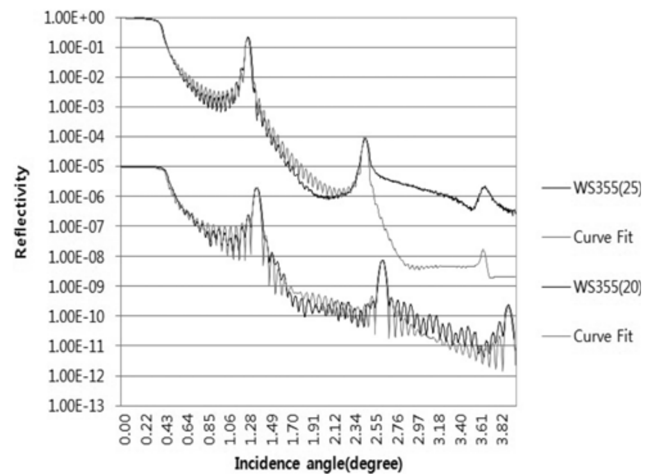

Fig. 3. Grazing incidence X-ray reflectivity of samples WS355(25) and WS335(20) (black line) and optimum curve fitting simulation (gray line) (the parameters of the simulations are listed in Table 5).

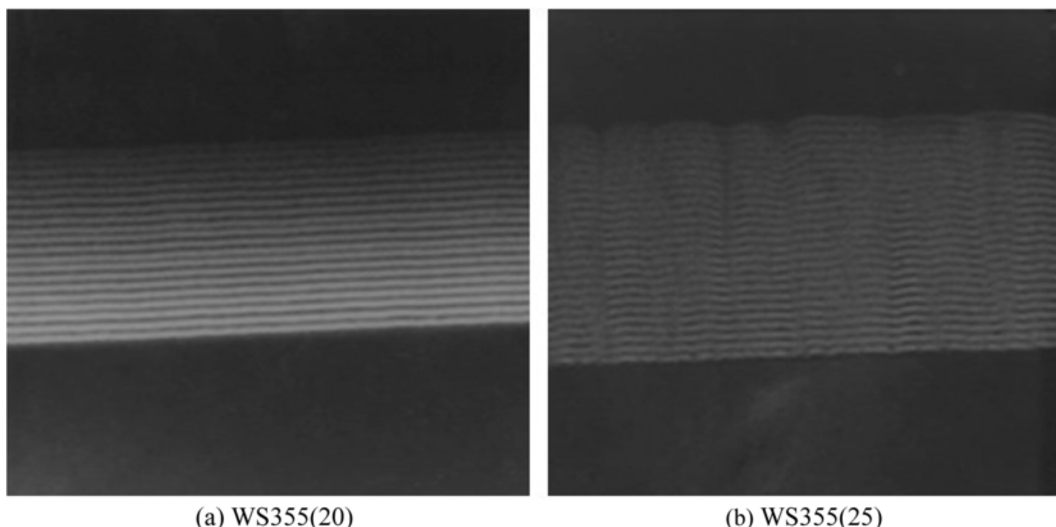

Fig. 4. Cross sectional TEM image of sample (a) WS355(20) deposited in the condition of abnormal glow, (b) WS355(25) deposited in the condition of normal glow in DC glow discharge (300 k xZoom).

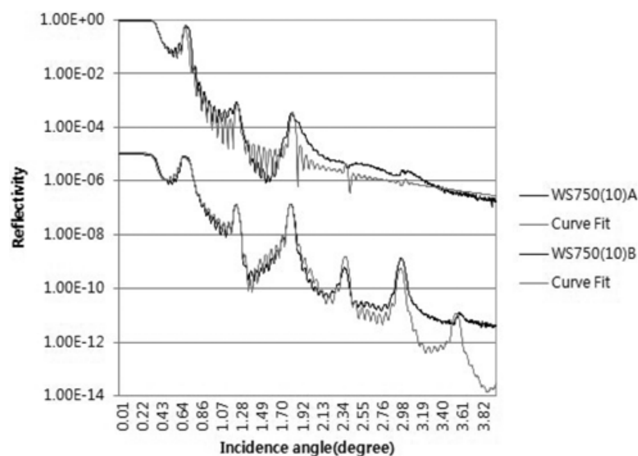

Fig. 5. Grazing incidence X-ray reflectivity of sample WS750(10)A and WS750(10)B (black line) and optimum curve fitting simulation (gray line) (the parameters of the simulations are listed in Table 5).

The result of XRR measurement and curve fitting for WS750(10)A and WS750(10)B is shown in Fig. 5. In WS750(10)A, reflectivity dramatically decreased as the incident angle was increasing. When the incident angle was more than 2°, a Bragg peak was not observed. On the other hand, a Bragg peak was found in case of WS750(10)B even when the incident angle was more than 3°.

In the simulation result of WS355(25) and WS750(10)A, interface roughness (σ) of 0.7-1.0 nm was confirmed. Interface roughness of 0.3-0.6 nm was identified for WS335(20) and WS750(10)B. Parameter values used for simulation are summarized in Table 6.

TEM images were used to confirm the results. TEM images of WS335(20) and WS750(10)B shown in Fig. 4(a) and Fig. 6(a) were not rougher than that of WS355(25) and WS750(10)A shown in Fig. 4(b) and Fig 6(b). Interface roughness was not increasing as the number of a bilayer from substrates was growing.

This result was because WS750(10)A and WS355(25) process were included in the normal glow discharge region in the I-V characteristics curve of DC glow discharge where the current increases and the voltage do not increase as power is increasing. The process condition of WS750(10)B and WS335(20) was included in the abnormal glow region where both the current and the voltage increase as power is increasing.

In the result of XRR and TEM analysis, interface roughness (σ) was increasing when a thin film multilayer was produced in the normal glow region.

3. Effect of the d-Spacing

The result of XRR measurement and curve fitting of WS390(20), WS380(20) and WS355(20) with varying d-spacing under the same process condition is shown in Fig. 7. Parameter values used for curve fitting are presented in Table 7. In the result of curve fitting, d-spacing was changed to 3.9 nm, 3.8 nm and 3.6 nm. Interface roughness was in the range of 0.3-0.6 nm, which was similar to WS720(10),

Table 6. Parameters for simulations of the X-ray reflectivity from samples WS355(25) and WS355(20) as shown in Fig. 3 and WS750(10)A and WS750(10)B as shown in Fig. 5 (parameters were obtained by Parratt32 software[16])

	Deposition conditions	Repetition (N)	d-Spacing (nm)	Gamma (Γ)	Surface Roughness and interface widths (σ) (nm)			
					Surface	Si on W	W on Si	Substrate
WS355(25)	Normal glow	25	3.62	0.64	1	0.7	1	0.5
WS355(20)	Abnormal glow	20	3.39	0.42	0.58	0.5	0.37	0.62
WS750(10)A	Normal glow	10	7.37	0.51	0.90	0.76	0.85	0.1
WS750(10)B	Abnormal glow	10	7.46	0.49	0.50	0.61	0.52	0.5

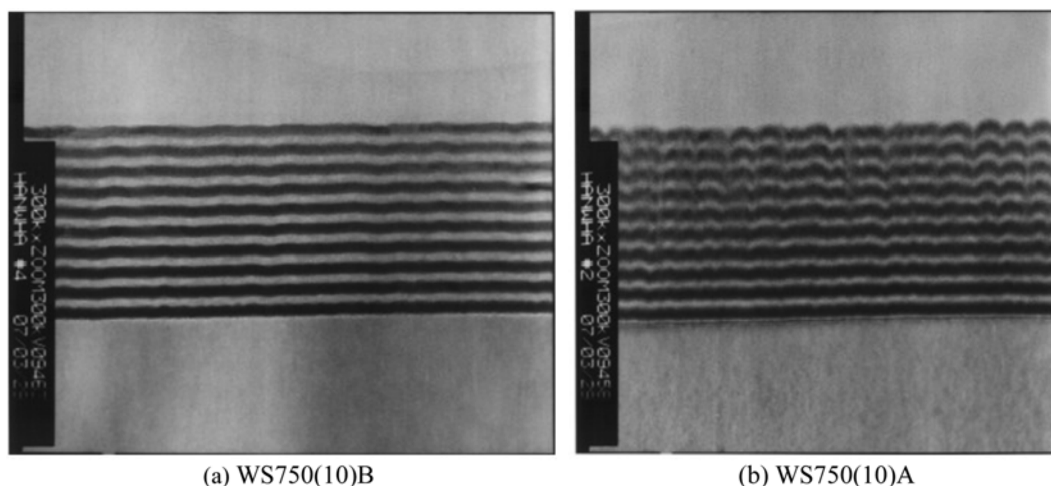

(a) WS750(10)B (b) WS750(10)A

Fig. 6. Cross sectional TEM image of samples (a) WS750(10)B and (b) WS750(10)A deposited in the condition of (a) abnormal glow and (b) normal glow in DC glow discharge.

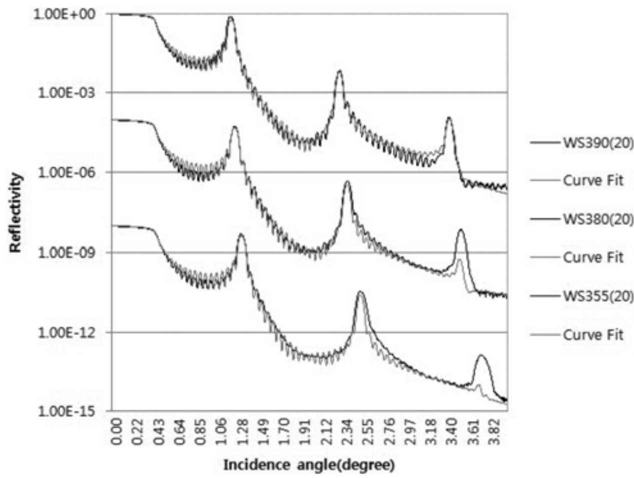

Fig. 7. Grazing incidence X-ray reflectivity of samples WS390(20), WS380(20) and WS355(20) (black line) and optimum curve fitting simulations (gray line) (the parameters of the simulations are listed in Table 6).

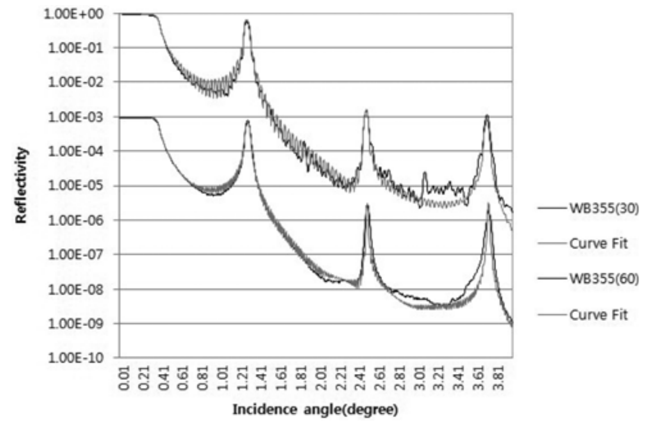

Fig. 8. Grazing incidence X-ray reflectivity of samples WB355(30) and WB355(60) to reflect 40, 50 keV hard X-ray (black line) and optimum curve fitting simulations (gray line) (the parameters of the simulations are listed in Table 7).

WS700(10), and WS680(10).

In reflectivity of the 1st Bragg peak, Cu characteristic X-ray reflectivity decreased by 25.92% as d-spacing diminished by 0.34 nm. The X-ray scattering rate increased due to roughness since d-spacing had decreased with same interface roughness.

According to the existing studies on interface characteristics of an Mo/Si multilayer, interface roughness changed depending on the deposition order during multilayer deposition. Roughness of Si deposition on Mo was lower than that of Mo deposition of Si [23-26]. However, in Tables 5, 6 and 7, similar roughness is shown in any interface regardless of W and Si deposition order. In addition, increase and decrease in multilayer interface roughness due to changes in d-spacing under the same sputter process condition were not observed.

Therefore, it was confirmed that surface and interface roughness during multilayer manufacture using a sputter was determined by deposition conditions but not layer thickness. Although layer thickness decreased under the same process condition, similar interface and surface roughness was maintained. It was confirmed that reflectivity decreased as an incident angle increased to reflect the same energy.

In this result, interface roughness of a multilayer was confirmed as an independent variable for d-spacing and this result accords with the previous study. Jensen et al. [9] deposited and analyzed the WC/SiC multilayer on a wafer substrate with 2-10 nm d-spacing.

4. Hard X-ray Mirror Production

A 3.55 nm d-spacing multilayer was designed to reflect hard X-rays of 40 keV and 50 keV at an incident angle of 0.25° and 0.20°, respectively. XRR graphs of two samples are shown in Fig. 8 and the result of curve fitting is summarized in Table 8. Interface roughness of two samples was 0.3-0.5 nm and Cu characteristic X-ray (Cu Kα, λ=~0.154 nm) reflectivity of WB355(30) and WB355(60) was 56.7% and 79.6%, respectively. The result of interface roughness was comparable to the study conducted by Paul and Lodha [27] that showed 0.35-0.43 nm interface roughness with a Pt/C multilayer deposited on a float glass substrate. It was a little higher than

Table 7. Parameters for simulations of the X-ray reflectivity from samples WS390(20), WS380(20) and WS355(20) as shown in Fig. 7 (parameters were obtained by Parratt32 software[16])

	Repetition (N)	d-Spacing (nm)	Gamma (Γ)	Surface Roughness and interface widths (σ) (nm)				Reflectivity of 1st Bragg Peak (%)
				Surface	Si on W	W on Si	Substrate	
WS390(20)	20	3.91	0.39	0.37	0.44	0.58	0.50	73.73
WS380(20)	20	3.78	0.37	0.37	0.54	0.58	0.50	53.33
WS355(20)	20	3.57	0.34	0.37	0.54	0.58	0.4	47.81

Table 8. Parameters for simulations of the X-ray reflectivity from samples WB355(30) and WB355(60) to reflect 40, 50 keV hard X-ray as shown in Fig. 8 (parameters were obtained by Parratt32 software[16])

	Repetition (N)	d-Spacing (nm)	Gamma (Γ)	Surface Roughness and interface widths (σ) (nm)				Reflectivity of 1st Bragg Peak (%)
				Surface	Si on W	W on Si	Substrate	
WB355(30)	30	3.57	0.48	0.50	0.35	0.42	0.44	56.71
WB355(60)	60	3.55	0.48	0.34	0.34	0.40	0.52	79.59

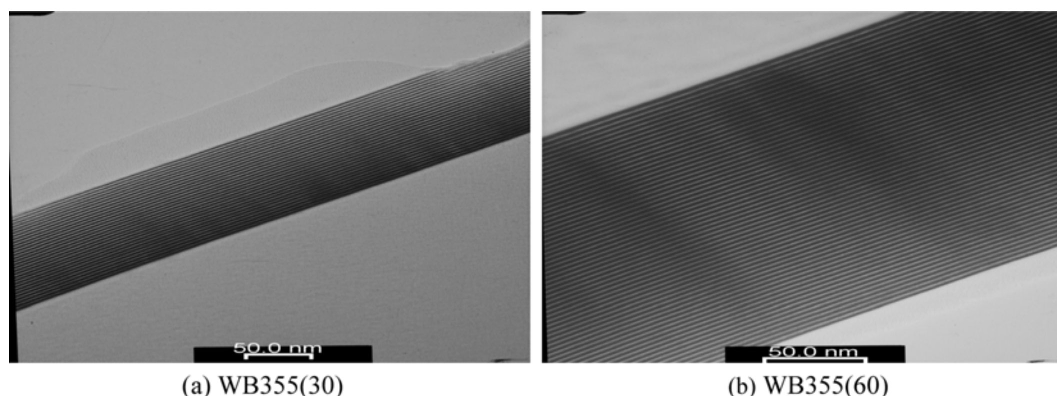

Fig. 9. Cross sectional TEM image of samples (a) WB355(30) and (b) WB355(60) to reflect 40 keV hard X-ray at 0.25 degree incident angle and 50 keV hard X-ray at 0.20 degree incident angle.

the study conducted by Windt et al. [28] that showed 0.23 nm interface roughness with a W/SiC multilayer deposited on a Si wafer. It may be caused by a difference between a Si wafer and a glass substrate.

Cross sectional TEM images of WB355(30) and WB355(60) are shown in Fig. 9. In two cross sectional TEM images, a clean interface is confirmed.

CONCLUSION

Interface roughness should be low in order to produce an excellent multilayer. When deposited on a substrate with same surface roughness under the same process condition, interface roughness was maintained regardless of a material type deposited and bilayer thickness.

When a deposition rate was reduced by lowering power to make a thin film in nm range thickness, sputtering appeared in the normal glow region so that interface roughness of a multilayer produced in this region was high. When samples were deposited in the abnormal glow region of DC glow discharge with power increase, a multilayer with excellent interface characteristics with low interface roughness was made.

Interface roughness increased and X-ray reflectivity decreased dramatically as substrate roughness was growing under the same material and process condition. Therefore, a substrate with low surface roughness should be used to make a multilayer with excellent interface characteristics. Low reflectivity could be improved by increasing the number of bilayers.

Cu characteristic X-ray (Cu Kα, λ=~0.154 nm) reflectivity was 79.6% in a 60-layer multilayer with d-spacing of 3.55 nm and 41.7% in a 60-layer bilayer of 2.3 nm. These multilayers can reflect hard X-rays of 20-60 keV at 0.25-0.45^o incident angle.

REFERENCES

1. E. Spiller, *Appl. Phys. Lett.*, **20**, 365 (1972).
2. Y. Jang, S. Park and K. Char, *Korean J. Chem. Eng.*, **28**(5), 1149 (2011).
3. J. Cho, S. Kim and K. Char, *Korean J. Chem. Eng.*, **20**(1), 174 (2003).
4. W. Chao, B. D. Harteneck, J. A. Liddle, E. H. Anderson and D. T. Attwood, *Nature,* **435**, 1210 (2005).
5. H. C. Kang, H. Yan, R. P. Winarski, M. V. Holt, J. Maser, C. Liu, R. Conley, S. Vogt, A. T. Macrander and G. B. Stephenson, *Appl. Phys. Lett.*, **92**, 221114 (2008).
6. C. Michaelsen, J. Wiesmann, C. Hoffmann, K. Wulf and L. Brugemann, *Proc. SPIE*, **4782**, 143 (2002).
7. M. R. Schuster, H. Goebel, L. Bruegemann, D. Bahr, F. Burgaezy, C. Michaelsen, M. Stoermer, P. Ricardo, R. Dietsch, T. Holz and H. Mai, *Proc. SPIE*, **3767**, 183 (1999).
8. Y. S. Park, S. J. Han, J. Y. Chae, C. K. Kim and K. S. Chon, *Proc. SPIE*, **7258**, 72583L (2009).
9. C. P. Jensen, K. K. Madsen and F. E. Christensen, *Exp. Astron.*, **20**, 93 (2005).
10. V. Cotroneo, R. Bruni, P. Gorenstein, G. Pareschi and S. Romaine, *Proc. SPIE*, **7437**, 74371Q (2009).
11. T. Salditt, D. Lott, T. H. Metzger, J. Peisl, G. Vignaud, P. Hoghoj, O. Scharpf, P. Hinze and R. Lauer, *Phys. Rev. B*, **54**, 5860 (1996).
12. E. E. Fullerton, J. Pearson, C. H. Sawers, S. D. Bader, X. Z. Wu and S. K. Sinha, *Phys. Rev. B*, **48**, 17 432 (1993).
13. S. P. Vernon, D. G. Stearns and R. S. Rosen, *Appl. Opt.*, **32**, 6969 (1993).
14. A. C. Thompson, J. Kirz, D. T. Attwood, E. M. Gullikson, M. R. Howells, J. B. Kortright, Y. Liu and A. L. Robinson, X-ray data booklet, 3rd Ed., Lawrence Berkeley National Laboratory, Berkeley, California (2009).
15. C. Braun, *Parratt32 Fitting routine for reflectivity data*, HMI, Berlin (1997).
16. L. G. Parratt, *Phys. Rev.*, **95**(2), 359 (1954).
17. D. Bahr and W. Press, *Phys. Rev. B*, **47**, 4385 (1993).
18. L. Névot and P. Croce, *Rev. Phys. Appl.*, **15**, 761 (1980).
19. S. K. Sinha, E. B. Sirota and S. Garoff, *Phys. Rev.*, **38**, 2297 (1988).
20. A. Grill, *Cold Plasma in Materials Fabrication: From Fundamentals to Applications*, Wiley, New York (1994).
21. M. Chládek, V. Valvoda, C. Dorner, C. Holý and J. Grim, *Appl. Phys. Lett.*, **69**, 1318 (1996).
22. V. Holý, J. Kuběna, W. W. van den Hoogenhof and I. Vávra, *Appl. Phys. A*, **60**, 93 (1995).
23. G. S. Elliot, A. D. Gromko, F. V. Veegaete, C. D. Johnson and D. C. Johnson, *Phys. Rev. B*, **58**, 8805 (1998).
24. H. J. Voorma, E. Louis, N. B. Koster and F. Bijkerk, *J. Appl. Phys.*,

83, 4700 (1998).
25. M. B. Stearns, C. H. Chang and D. G. Stearns, *J. Appl. Phys.*, **71**, 187 (1992).
26. D. L. Windt, R. Hull and W. K. Waskiewick, *J. Appl. Phys.*, **71**, 2675 (1992).
27. A. Paul and G. S. Lodha, *Phys. Rev. B*, **65**, 245416 (2002).
28. D. L. Windt, S. Donguy, C. J. Hailey, J. Koglin, V. Honkimaki, E. Ziegler, F. E. Christensen, C. M. Hubert Chen, F. A. Harrison and W. W. Craig, *Proc. SPIE*, **4851**, 639 (2003).